



# Characterization of Unsteady Combustion Phenomena in a University Scale Rocket Combustor

Abhinav Dasari\* and Mirko Gamba†

*The University of Michigan, Department of Aerospace Engineering, 1320 Beal Avenue, Ann Arbor, MI 48109*

We investigate the steady and unsteady flame properties in a moderate pressure, single shear coaxial injector operated with gaseous oxygen/hydrogen and how they relate to the underlying fluid dynamic properties of the flowfield. Under a certain range of conditions, we observe strong modifications of the flame structure as a result of a low-amplitude thermoacoustic instability that develops naturally under fuel-lean conditions. In particular, we observe a periodic evolution of the flame front where ejection events are followed by near-complete extinction and re-ignition. To link the onset of the thermoacoustic instability under fueled (reacting) conditions to the fluid dynamics of the system, we conduct corresponding mixing studies of variable density, non-reacting shear coaxial jets. We particularly investigate the onset and properties of self-excited hydrodynamic instabilities that are observed at high inner-to-outer jet momentum flux ratios. We thus attempt to link them to the unsteady behavior of the corresponding reacting cases.

## Nomenclature

$S$	Density ratio
$R$	Velocity ratio
$Re$	Reynolds number
$At$	Atwood number
$M$	Mach number
$\phi$	Equivalence Ratio
$J$	Momentum flux ratio
$\theta$	Momentum thickness
$\rho$	Density
$v$	Velocity
$D$	Diameter

### *Subscript*

$i$	Inner stream
$o$	Outer stream
$j$	Jet exit
$\infty$	Ambient fluid surrounding jets

## I. Introduction

The understanding of unsteady combustion processes, including combustion instabilities and flame stabilization are of critical importance to the design of modern combustors. Observations from some of our earlier and current experiments at the Michigan Single Element Injector Facility<sup>1</sup> established a relation between the

\*Graduate Student, Department of Aerospace Engineering, 1320 Beal Ave., University of Michigan, Ann Arbor, MI 48109, Student Member AIAA.

†Assistant Professor, Department of Aerospace Engineering, 1320 Beal Ave., University of Michigan, Ann Arbor, MI 48109, Member AIAA.

velocity difference of shear coaxial propellant streams and the flame lift-off in the moderate-pressure combustor. Furthermore, experiments at fuel lean conditions also demonstrated the presence of a self-sustained, unsteady combustion at moderate pressures in the combustor.<sup>2,3</sup> Further experiments to better understand the mixing properties in the shear coaxial propellant streams configuration led to the observation of self-excited instabilities in the coaxial jet column and the formation of so-called *side jets*: radial ejections of jet fluid. The side jets are observed under certain flow conditions, they have a periodic behavior and their general structure appears to be visually similar to that of the unsteady flames of corresponding reacting cases that motivated the study in the first place. This led to formulating the hypothesis that a coupling exists between the self-sustaining combustion instability, which are believed to be thermoacoustic in nature, and absolute instabilities<sup>4</sup> in variable-density jets. The present work aims to study variable-density coaxial jets and their stability properties in greater detail to assess if hydrodynamic instabilities could in fact be linked to the observed flame structure and thus the onset of the thermoacoustic instability.

Hydrodynamic instabilities and the formation of side jets in variable-density round jets have been studied in the past. Preliminary experimental investigations by Sreenivasan, Raghu and Kyle<sup>5</sup> based on earlier theoretical work showed that round jets of different densities issuing into ambient (still) air exhibit two types of behavior depending on the density ratio  $S = \rho_j/\rho_\infty$  between the jet and ambient fluids, one possibly corresponding to an absolute instability and the other one to a convective instability. The possibility of a change in the nature of the instability from absolute to convective was also proposed. Flow visualization techniques were used to reveal intermittent breakdown and spectacular spreading of low density jets. For their experiments, based on the theory by Monkewitz and Sohn,<sup>6</sup> they considered  $S$  and Mach number  $M$  to be the most important parameters. The theory is linear and neglects viscous and buoyancy effects. Results from the experiments and theory showed similar trends, but there were differences in the experimentally observed and theoretically predicted stability regimes, which were attributed to the use of a small nozzle diameter in the experiments. The Monkewitz-Sohn theory also predicts that the helical mode in an absolutely unstable jet is significantly more stable than the axisymmetric mode.

Heated axisymmetric jets in the translational regime discharging into cold air were used to demonstrate that for low Reynolds number  $Re$  and  $S$  below 0.7, global oscillations of the jet become self-excited, an effect that is related to local absolute instability.<sup>7</sup> Linear stability analysis by Monkewitz and Sohn<sup>6</sup> revealed that the instability could change from convective to absolute as the local value of  $S$  was decreased. For an inviscid, ideal gas, neglecting buoyancy and viscous effects, they found the highest  $S$  for absolute instability to be about 0.72, for a zero  $M$ , axisymmetric case with a vorticity thickness of 8.7% of the local jet diameter.

In a later study, Kyle and Sreenivasan<sup>8</sup> observed two kinds of instabilities in the near field. The first was an intense oscillatory instability when  $S$  was less than 0.6, whose overall behavior was shown to depend only on  $S$  and  $(D_j/\theta)$ , and was found to be independent of  $Re$  in the cases considered. When  $S$  was more than 0.6, shear layer fluctuations evolved similar to constant-density jets. For the experiments,  $M$  was limited to below 0.3 to neglect compressibility effects. Buoyancy effects were negligible. Their analysis suggested that all non-dimensional characteristics of the flow should depend primarily on the global parameters  $D_j/\theta$ ,  $S$  and  $Re$ .

Singh, Sundararajan and Kyle<sup>9</sup> developed a finite element model for a confined variable-density jet and studied the effects of aspect ratio,  $S$  and jet location. They found that aspect ratio and  $S$  were the main parameters controlling entrainment and mixing and were responsible for causing instability and recirculation within the mixing tube.  $Re$  was not found to have any significant effect over entrainment ratio. Entrainment increased for short distances and decreased for larger distances when the jet was moved away from the inlet. Mixing between jet and entrained fluid was seen to improve when jet was moved away from the tube inlet.

Nichols, Schmid and Riley<sup>10</sup> showed that the presence of buoyancy caused a more abrupt transition to turbulence, which helps explain differences between normal and microgravity diffusion flames. Wang et al.<sup>11</sup> performed large eddy simulations of weakly confined turbulent variable-density jets with different  $S$  and  $Re$  values, and observed “*long-finger shaped streamwise vortices, regularly arranged along jet nozzle lip*”<sup>11</sup> in the lowest  $S$  case (corresponding to injection of helium into ambient air).

Gerashchenko, Charonko and Prestridge<sup>12</sup> experimentally studied the velocity and density statistics for variable-density mixing of a heavy fluid jet with lower density ambient fluid. The effects of buoyancy could not be neglected in their experiments, and this effect was found to be important for most turbulent quantities measured. High  $At$ , high  $Re$  cases were seen to have a reduced lateral spread compared to low  $At$ , low  $Re$  cases.

Most work done on variable-density jets points towards  $S$  being the dominating parameter (in the limit

$M \rightarrow 0$ ). Varying  $Re$  does not seem to have any significant effect on most earlier experiments. In confined jets, aspect ratio was an important parameter as well. Earlier investigations were performed in the regime where buoyancy could be neglected, but later studies found buoyancy to be an important factor in determining the properties of turbulence. Theoretically, experimentally and computationally, variable-density round jets discharging into ambient fluids have been studied in great detail. On the contrary, less work has been done on understanding variable-density round jets in co-flowing streams, and no studies of variable-density effects in coaxial injectors are available in the literature. This work described here aims to be the starting point for developing a better understanding of variable-density coaxial jets and their link to the study and improved understanding of unsteady combustion processes in this injector configuration.

The work that we consider here is based on a confined shear coaxial round jet stream where the inner and outer fluids were chosen to generate different cases. In the single stream configuration, the main parameter controlling the stability properties is the density ratio. However, in the coaxial configuration, a second parameter now becomes relevant: the inner-to-outer velocity ratio  $R$ . Therefore, we here investigate the flowfield and stability of coaxial jets as a function of both  $S = \rho_i/\rho_o$  and  $R = v_i/v_o$  by performing non-reacting mixing studies. In particular, we use planar laser-induced fluorescence (PLIF) imaging of a fluid tracer seeded into one of the two streams to identify the structure and quantify the mixing properties of the coaxial jet. We will particularly focus on investigating the morphology of the coaxial jets, the onset of side jets and any other property relevant to the identification of any unsteady behavior of the system.

## II. Experimental Setup

The Michigan Single Element Injector Facility was used for performing experimental measurements to study the mixing and instabilities in non-reacting coaxial jets, as well as the corresponding reacting studies.<sup>3</sup> The experimental configuration and diagnostic techniques used in this study are described in this section.

### A. Test Apparatus

The Michigan Single Element Injector Experiment, originally designed and sized by Schumaker<sup>1,13</sup> based on work done at Penn State and NASA Marshall,<sup>14-16</sup> is a laboratory scale gas phase rocket engine capable of operations at chamber pressures up to 10 atmospheres. The facility was originally developed to study mixing in reacting and non-reacting coaxial jets, and has been described in detail by Schumaker.<sup>1</sup> A schematic diagram of the facility is shown in Figure 1(a).

The modular rocket combustor has optical access windows for laser-based diagnostics, an injection block with a single shear coaxial jet injector located at its center, and an actively cooled nozzle block. It is machined out of C145 Tellurium-Copper. Figure 1(b) is a schematic layout of the coaxial jet, highlighting some of its fluid dynamic features. The chamber itself has a square cross section of 50.8 mm  $\times$  50.8 mm (with rounded corners) with a maximum length of 267 mm, and is composed of several instrumented, interchangeable modules. The total length of the chamber can be varied based on the number of modules used. The water-cooled nozzle block terminates the chamber. As the entire engine is not actively cooled, the heating capacity of the thermal mass of the engine limits the test time during reacting cases. The external temperature of the engine is monitored by K-type thermocouples, and the temporal evolution of pressure is monitored using a Kistler 6061B and a Cooper PTG-404-A pressure transducers. Data from the transducers is acquired at 10 kHz.

A 90 mm long section with quartz windows on all sides provides optical access to the chamber. There are two narrow windows for laser access on a set of opposite sides, while the two other sides house full-width windows for imaging. Being modular the optical section can be placed at different longitudinal positions, to characterize different flame regions. For the purpose of this present work, the section was always placed at the base of the chamber, immediately downstream of the injector.

The injector block can house coaxial propellant delivery tubes of different inner and outer diameters to facilitate operation over a range of conditions. For reacting cases, the inner tube delivers the oxidizer ( $O_2$ ) and the surrounding annulus delivers the fuel ( $H_2$ ). For studies involving mixing in variable density jets, inert gases like He,  $N_2$  and Ar are used, and the required gases are injected through either the inner tube or the surrounding annulus depending on the density ratio required. For all cases in the present study, the inner tube has an inner diameter  $D_i$  of 3.66 mm and an outer diameter of 4.76 mm, and the annulus has a diameter  $D_o$  of 6.73 mm.

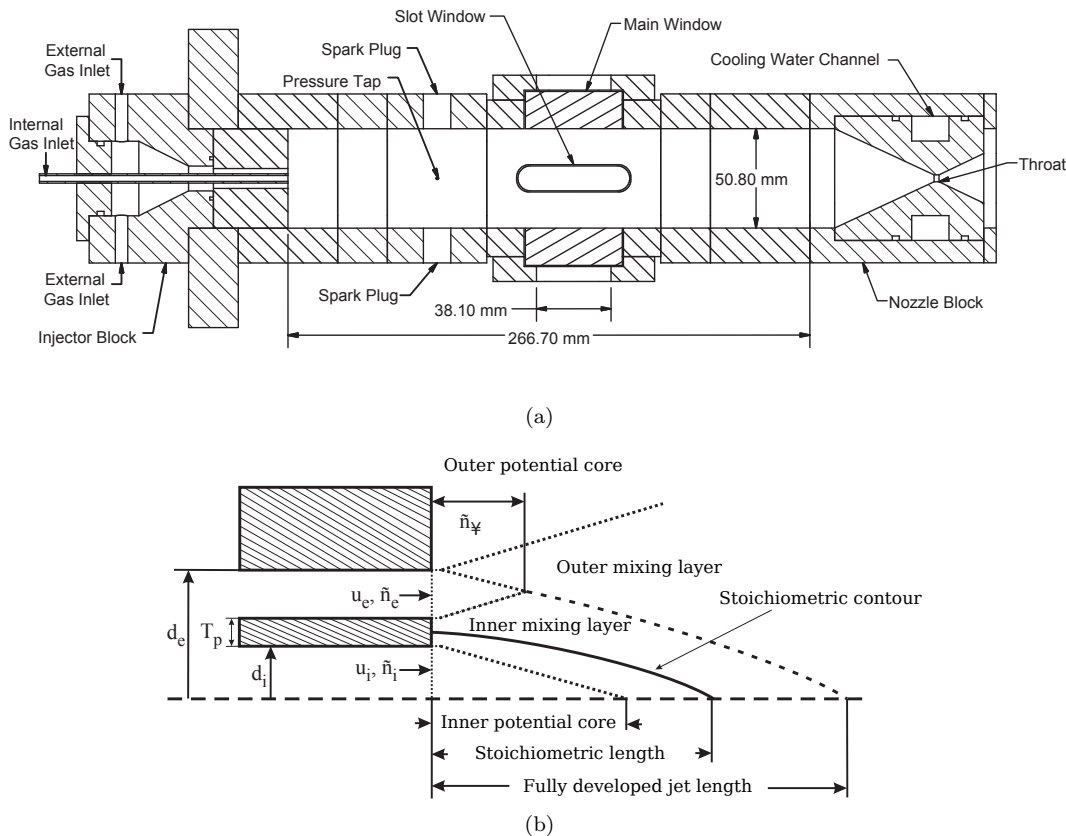


Figure 1. (a) Schematic diagram of the Michigan Single Element Injector Facility, and (b) of the shear coaxial jet. From Schumaker (2009)<sup>17</sup>

The gases are delivered to the rocket chamber by a set of remotely operated solenoid valves. A system of pressure regulators, needle valves, choked orifices and pressure transducers is used to regulate the mass flow rates. The entire system is controlled by a LabVIEW-based controller.

## B. PLIF System

In reacting cases, the instantaneous location of the reaction zone is approximately marked by OH PLIF, while the overall flame structure is imaged by detecting OH\* chemiluminescence. A typical system with a tunable dye laser (Continuum ND 6000) pumped by the second harmonic of a Nd:YAG laser (Spectra Physics Pro 250) is used to excite the A-X(1,0)  $Q_1(7)$  transition line of OH near 283 nm. An intensified CCD camera (Andor iStar), equipped with a 100F/2.8 UV lens is used to carry out the fluorescence imaging. The camera is arranged with its line-of-sight perpendicular to the propagation of laser sheet through the combustor. The field of view is approximately 44 mm  $\times$  44 mm. The ICCD camera is gated to 200 ns and a 310 nm ( $\pm 10$ nm) bandpass filter is used to block unwanted light. With run times of 12 seconds and a frame rate of 5 Hz, at least 30 useful images are captured during each run, after dropping data from the initial startup transients. Standard background and sheet correction schemes<sup>18</sup> using dilute toluene in the chamber are implemented to account for non-uniformities in the laser sheet energy distribution.

Chemiluminescence imaging is done with a high speed CMOS camera (Phantom v771 and Phantom v9.1) equipped with a Nikon 50F/1.8 lens at 10 kHz.

## C. Toluene PLIF System

For the non-reacting mixing studies, seeded tracer-based PLIF was used to measure the mole fraction distribution of one of the two streams in variable-density jets. In particular, we used toluene as the tracer species due to its good fluorescence properties.<sup>19,20</sup> Toluene absorbs at 266nm, making it a good tracer for use with Nd:YAG lasers, and provides strong fluorescence signals. For the measurement reported here, one of the two

Table 1. Combination of gases used to generate different density ratios for non-reacting mixing studies in variable-density coaxial jets.

Inner Jet	Outer Jet	$S$
He	N <sub>2</sub>	0.14
N <sub>2</sub>	Ar	0.70
N <sub>2</sub>	N <sub>2</sub>	1.00
Ar	N <sub>2</sub>	1.43
N <sub>2</sub>	He	6.99

gas streams is saturated with toluene by bubbling a known mass flow rate through a toluene seeder. The illumination is provided by the fourth harmonic of a Nd:YAG laser (Spectra Physics Pro 250), and the LIF signal is captured with an electron multiplying CCD camera (Andor iXon), equipped with a 100F/2.8 UV lens and a 310 nm ( $\pm 10nm$ ) bandpass filter is used to block scattered light and other background light. The electron multiplication feature on the EMCCD camera was disabled because sufficient signal was achieved without it. The toluene concentrations used in these experiments were high enough to cause appreciable absorption of the laser intensity between the edges of the interrogation volume. To compensate for this, a Beer's Law absorption correction scheme that uses a ray-tracing algorithm is applied to the processed images. Standard background and sheet correcting schemes are also applied.

#### D. Test cases

Past work at this facility<sup>1,13</sup> focused on steady, rich cases. Recent experiments to understand the conditions under which steady, attached and lifted flames could exist also showed that self-sustaining unsteady flames, with low amplitude instabilities could exist under fuel-lean conditions.<sup>2,3</sup>

For the reacting cases, gaseous oxygen and hydrogen were used. Tests were run both at atmospheric and higher pressure (i.e., with the nozzle attached). Runs were made at different equivalence ratios and mass flow rates. We particularly focus on near-stoichiometric and fuel-lean cases. For most cases, the inner stream Reynolds number  $Re_i$  varies from 11000 to 25000 and the outer stream Reynolds number  $Re_o$  varies from 700 to 3000. Fuel-to-oxidizer velocity differences  $\Delta v$  range from -45 m/s to 27 m/s and  $R$  varies from 0.12 to 1.64. A more comprehensive set of measurements and cases are considered in our companion work.<sup>3</sup>

For non-reacting cases,  $S$  and  $R$  are the main parameters considered in the present study. Different density ratios are obtained by injecting suitable gases into the inner tube and the surrounding annulus. Experiments are performed at  $S$  of 0.14, 0.7, 1, 1.43 and 6.99. Table 1 gives a summary of the gas combinations used for different  $S$ . For each  $S$ ,  $R$  values of 0.5, 0.7, 1, 3.5, 6 and 9 are considered. For the range of these parameters considered here,  $Re_i$  varies from about 700 to 40000, and  $Re_o$  varies from 200 to 6000. Seeding with toluene would cause a small change in the density of the seeded stream, but that change is neglected here while calculating the density ratios.

For reacting cases, the run time of the rocket is limited to 12 seconds to avoid overheating of the rocket beyond its maximum tolerable temperature. Non-reacting cases are not limited by rocket heating and data is collected over a period of 30 seconds. In both cases, the data is collected after the start-up transients have terminated.

### III. Results and Discussions

#### A. Reacting cases: flame structure under unsteady operation

Figure 2 shows a map of the liftoff stability of the O<sub>2</sub>/H<sub>2</sub> shear coaxial jet flame as a function of the equivalence ratio  $\phi$  and the fuel-to-oxidizer velocity difference  $\Delta v = v_o - v_i$ . This figure was compiled from data generated in current and concurrent studies, and from previous work done at the same facility<sup>1,2,17</sup> for gaseous O<sub>2</sub>/H<sub>2</sub> cases, both with and without the nozzle.  $\Delta v$  was used to correlate the data since it was found to best separate the lifted from the attached cases as seen in the figure.

Previous work done at this facility<sup>17</sup> considered very rich mixtures; more recent<sup>2</sup> and present<sup>3</sup> works concentrate on near-stoichiometric and fuel-lean mixtures, which are usually used in actual operation. Keep-

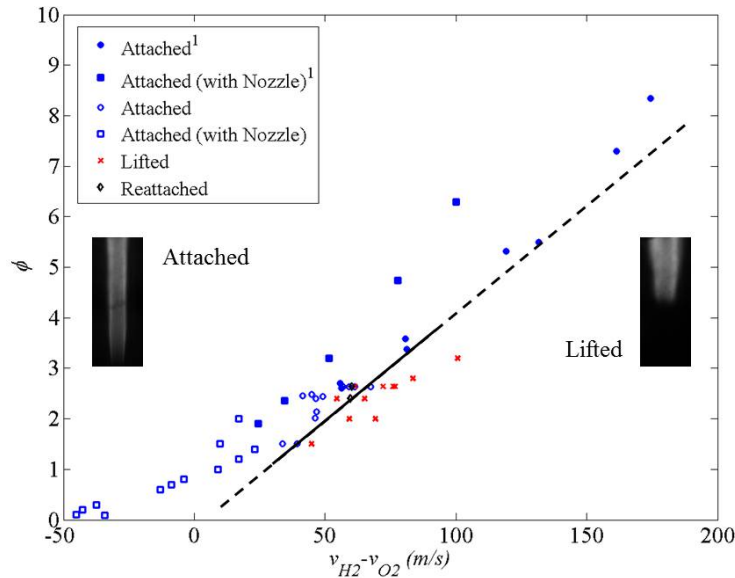


**Figure 2. Liftoff Stability map for  $O_2/H_2$  shear coaxial turbulent jet flame: dependence on equivalence ratio and fuel-oxidizer velocity difference. Insets are long exposure  $OH^*$  chemiluminescence images of an attached and lifted case respectively. <sup>1</sup>Data from Schumaker<sup>1</sup>**

ing the total mass flow rate constant, going fuel lean is observed to make the flame go unsteady. Figure 3 compares the visible structure of an unsteady flame and a steady, attached flame, as they are referred to in the present work. The attached case is stable and shows an elongated and orderly global flame, while the lean case shows a shorter, broader and unsteady flame structure. Visual inspection of the temporal behavior, backed by pressure data, indicates that the flame goes through repeated cycles of growth, contraction, extinction and reignition over the test time. Even though the amplitude of the pressure fluctuation is small, the impact on global flame structure and its stability is significant.

A sequence of uncorrelated instantaneous  $OH$  PLIF images for a case with  $\phi = 0.3$  and  $\Delta v = -38$  m/s is presented in Figure 4. The PLIF sequence is extracted from the same run at different stages of the growth cycle but it does not correspond to any particular sequence. Multiple flame fronts are observed in the instantaneous images: an inner reaction layer associated with the  $O_2/H_2$  boundary and an outer layer associated with the  $H_2$  stream and the oxygen-rich outer recirculation zones formed by post-combustion gases of the inner flame. A similar cyclical structure is observed from the high-speed chemiluminescence movies collected with the  $OH$  PLIF images. The most important feature is the periodic evolution of the flame front: The flame is observed to pulsate generating a vortex-like structure, creates a strong ejection, and then it collapses to nearly extinguish just to reignite and repeat the cycle thereafter. Motivated by this periodic behavior, the following mixing studies were conducted.

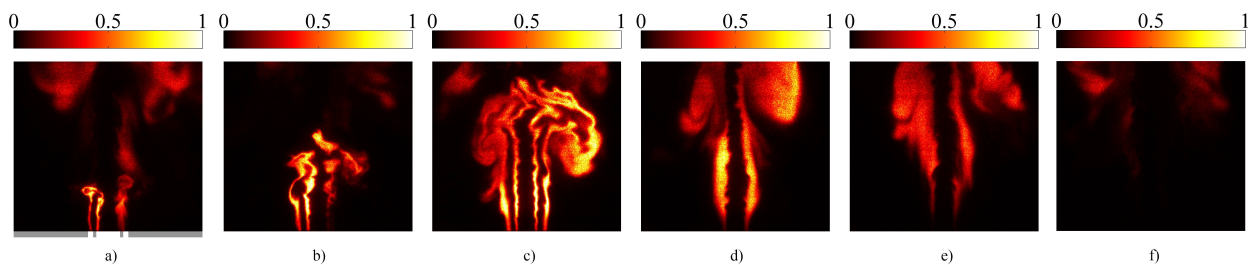
## B. Non-reacting cases: the onset of instabilities and side jets

Figure 5 shows example of the measured mole fraction of one of the two streams using the toluene PLIF technique. The case shown in Figure 5(a) refers to a stable case where no oscillatory behavior or formation of side jets is observed. The general structure of the coaxial jets is that of a typical axisymmetric shear layer. In this particular case, the inner (turbulent) jet is found to persist for many jet diameters, while the outer annulus is quickly entrained into the inner jet and breaks down. On the contrary, Figure 5(b) shows a case where the combination of parameters ( $S, R$ ) is such that side jets occur. In this study, a side jet is defined as a self-excited, periodic radial ejection or spreading from the jet, and it is possibly related to a local absolute instability.

Figures 6 and 7 show two sets of consecutive toluene PLIF frames (acquired at 5 Hz) for the cases without ( $S = 1.43$  and  $R = 1$ ) and with ( $S = 6.99$  and  $R = 6$ ) side jet formations. Although the images in the two sets are not time resolved to capture the temporal evolution of the system, they demonstrate that the flowfield in cases where no side jets are found is stationary, whereas for the case with the formation of side



**Figure 3.** Long exposure picture of (a) unsteady (b) steady attached flames. (Note: the two horizontal bands in the middle of flame in image (a) are reflections of the hot injector on the back window.



**Figure 4.** PLIF images for an unsteady flame showing a sequence of 6 instantaneous images. The position of the coaxial injector is shown in image (a). The relatively darker region at the bottom of the image is due to reflections from the injector block.

jets the other jet becomes very unsteady: side jets are formed on both (visible) sides, they fluctuate and the core itself tends to break down randomly. Furthermore, by looking at the instantaneous images of the case with side jets present (figure 7), it appears that the side jet are associated with an azimuthal instability which induces a rotation of the outer jet and of the side jets in particular, around the central stream. More specifically, we can infer the rotational motion by noting that in figure 7c through 7f, the outer stream in both the near- and far-fields becomes visible at alternating sides of the coaxial jet where the side jet is present.

Figures 6 and 7 are just two examples showing the existence or absence of side jets. In order to investigate the conditions ( $S$ ,  $R$  pair) under which side jets are found, we investigated a range of values of  $R$  and  $S$ . Figures 8 and 9 depict the qualitative evolution of the coaxial jet flowfield and the character of the instability as one of the two parameters is varied while the other is held constant. In these figures, the top row of images refers to instantaneous values, while the lower row is a time average distribution. It has to be noted that for certain experimental conditions in which the inner stream was seeded, getting a quantitative result was found to be difficult due to the laser and fluorescence reflections from the bottom wall. To reduce the effect of reflections on image correction schemes, the bottom portion of the image was removed from the field, which resulted in insufficient data for proper normalization based on the outer core regions for proper computation of the mole fraction. Examples of these cases are the cases shown by figure 9a and 9c. As a result, some of the fields are presented only for qualitative comparison to show the changes in the flowfield structure. Note also that the average images were obtained by ensemble-averaging 150 instantaneous images to reduce statistical error.

Figure 8a through 8f show a set of instantaneous images of the mole fraction of the outer jet as  $S$  is held constant to 0.142 while  $R$  is varied from 0.5 to 9. With increasing  $R$ , the length of the inner (unmixed) core increases, while the break down of the outer annulus occurs at an increasingly smaller distance from the exit plane (figure 8g through 8l). From the instantaneous images, it is also apparent that side jets begin to

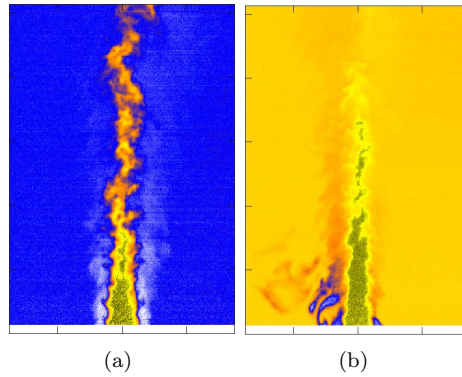


Figure 5. Toluene PLIF images of typical cases (a) without and (b) with side jets.

appear at some value of  $R$  and, with increasing  $R$ , they tend to extend less in the axial direction.

Figure 9 shows the change in structure when  $R$  is held constant to a value of 3.5 while  $S$  is varied from 0.143 to 6.99. Side jets appear in the instantaneous images for higher values of  $S$  (figure 9a through 9e). Contrary to the case of Figure 8, the inner and outer core lengths remain nearly the same, increasing only slightly from figure 9f through 9j as a result of increasing  $S$ . Higher values of  $S$  also seem to cause the side jets to propagate more in the axial direction (i.e., to occur further downstream of the exit plane).

A preliminary study on the effects of Reynolds number on the observed trend (specifically for the case at  $S = 6.99$  and  $R = 6$ ) was also carried out. Experiments at two different flow rates ( $Re_i$  and  $Re_o$ ) were conducted, but insignificant difference in the instantaneous or average flow structures are found. This observation, however, needs to be validated with further experiments to generate a more complete understanding of Reynolds number effects.

Inner-to-outer momentum flux ratio  $J = SR^2$  is an important parameter in variable-density jets. Villiermaux and Rehab<sup>21</sup> hypothesized that the effects of variable-density jets on mixing could be accounted for by this parameter. In the context of coaxial turbulent jets, Schumaker and Driscoll<sup>22</sup> reported that the stoichiometric centerline mixing lengths in non-reacting cases were proportional to the square-root of  $J$ . In an attempt to collapse the  $S$  and  $R$  dependence of the formation of side jets, we describe the presence of this flow feature with  $J$ . Thus, Figure 10(a) shows a map of all non-reacting cases considered in this study as a function of  $S$  and  $R$ . Each symbol in the map correspond to a case ( $S, R$  pair). The round (red) symbols indicate cases where side jets were observed, while the square (blue) symbols indicate cases when they were not observed. We can immediately note that the cases with side jets lay in the upper right corner. A line of constant momentum flux ratio  $J$  is seen to separate the regions of cases with and without side jets, points above the line being those with side jets present. Figure 10(b) is an alternative representation of the data presented in Figure 10(a): all data points are described by their value of  $J$  and the y-axis indicates the presence of side jets (value of 1) or not (value of 0). The figure shows that there exist a well defined value of  $J$  that divides the two regimes, In particular for the current study, side jets are seen to be present in cases with  $J$  larger than about 10. The region between  $J = 10$  and 20 is possibly a region of transition between the two regimes. In general, however, the presence or absence of side jets is very consistent and well-defined. Past experiments in this facility<sup>17</sup> were limited to values of  $J$  below 10, and the appearance of side jets and/or other instabilities was not mentioned, which is consistent with the findings of this study.

#### IV. Conclusion and Outlook

Shear coaxial  $\text{GH}_2/\text{GO}_2$  jet flame experiments performed at the Michigan Single Element Injector Facility show the presence of self-sustaining unsteady combustion at fuel lean, elevated pressure cases. OH PLIF image sequences of this unsteady combustion, though not time resolved, illustrate the periodic variability of the flame front shape and location.

Non-reacting experiments with different inner-to-outer stream density and velocity ratios show the presence of self-excited instabilities that results in side jets at higher values of density and velocity ratios. It is found that the dependence on both parameters ( $S, R$ ) can be reduced to a single parameter by defining an



inner-to-outer momentum flux ratio  $J = SR^2$ . For value of  $J$  larger than about 15, variable-density coaxial jets are found to have some form of instability and/or the formation of side jets.

Future work at this facility intends to study the self-sustaining, unsteady combustion phenomena in both attached and lifted flames, in addition to flame stabilization processes. For non-reacting cases, the dependence of side-jets on other parameters such as buoyancy and Reynolds number remains to be explored. High speed Toluene PLIF imaging is expected to provide a better understanding of the evolution and structure of side jets. The ultimate aim is to explore the relationship between thermoacoustic instabilities in reacting cases and hydrodynamic instabilities in non-reacting cases. Study of combustion in variable-density jets and development of a theoretical model for instabilities in variable-density coaxial jets are also proposed.

Implementing simultaneous PLIF and PIV measurements, which is our short term goal, would help produce time resolved measurements of flame location and flowfield properties during the relevant unsteady combustion processes.

## Acknowledgments

The authors would like to thank Dr. Campbell D. Carter, Air Force Research Laboratory, Wright-Patterson Air Force Base, OH for lending the Andor iXon EMCCD camera. The authors also wish to acknowledge Logan W. White for his help, suggestions and the stimulating discussions throughout the course of this study. This work is supported by NASA Marshall Space Flight Center under grant no. NNM13AA11G with P. Kevin Tucker as Technical Mentor.

## References

- <sup>1</sup>Schumaker, S. A., *An Experimental Investigation of Reacting and Nonreacting Coaxial Jet Mixing in a Laboratory Rocket Engine*, Ph.D. thesis, University of Michigan, Ann Arbor, 2009.
- <sup>2</sup>Dasari, A., White, L. W., Abul-Huda, Y. M., and Gamba, M., "Experimental Characterization of the Flowfield and Flame Structure in a Rocket Combustor Using OH-PLIF," *Proceedings of the Combustion Institute - Canadian Section*, Windsor, CA, 2014, p. 6.
- <sup>3</sup>Dasari, A., White, L. W., and Gamba, M., "Investigation of Instability Mechanisms in a Laboratory Scale GH<sub>2</sub>/GO<sub>2</sub> Combustor," *To be presented at the 2015 AIAA SciTech Conference*, 2015.
- <sup>4</sup>Huerre, P. and Monkewitz, P. A., "Absolute and convective instabilities in free shear layers," *Journal of Fluid Mechanics*, Vol. 159, 1985, pp. 151–168.
- <sup>5</sup>Sreenivasan, K. R., Raghu, S., and Kyle, D. M., "Absolute instability in variable density round jets," *Experiments in Fluids*, Vol. 7, No. 5, 1989, pp. 309–317.
- <sup>6</sup>Monkewitz, P. A. and Sohn, K. D., "Absolute instability in hot jets," *AIAA Journal*, Vol. 26, No. 8, Aug. 1988, pp. 911–916.
- <sup>7</sup>Monkewitz, P. A., Bechert, D. W., Barsikow, B., and Lehmann, B., "Self-excited oscillations and mixing in a heated round jet," *Journal of Fluid Mechanics*, Vol. 213, 1990, pp. 611–639.
- <sup>8</sup>Kyle, D. M. and Sreenivasan, K. R., "The instability and breakdown of a round variable-density jet," *Journal of Fluid Mechanics*, Vol. 249, 1993, pp. 619–664.
- <sup>9</sup>Singh, G., Sundararajan, T., and Shet, U. S. P., "Entrainment and Mixing Studies for a Variable Density Confined Jet," *Numerical Heat Transfer, Part A: Applications*, Vol. 35, No. 2, Feb. 1999, pp. 205–224.
- <sup>10</sup>Nichols, J. W., Schmid, P. J., and Riley, J. J., "Self-sustained oscillations in variable-density round jets," *Journal of Fluid Mechanics*, Vol. 582, 2007, pp. 341–376.
- <sup>11</sup>Wang, P., Fröhlich, J., Michelassi, V., and Rodi, W., "Large-eddy simulation of variable-density turbulent axisymmetric jets," *International Journal of Heat and Fluid Flow*, Vol. 29, No. 3, June 2008, pp. 654–664.
- <sup>12</sup>Gerashchenko, S., Charonko, J. J., and Prestridge, K., "Simultaneous PIV and PLIF measurements for the study of variable density turbulent mixing," *17th International Symposium on Applications of Laser Techniques to Fluid Mechanics*, Lisbon, Portugal, 2014, p. 11.
- <sup>13</sup>Schumaker, S. A. and Driscoll, J. F., "Mixing properties of coaxial jets with large velocity ratios and large inverse density ratios," *Physics of Fluids (1994-present)*, Vol. 24, No. 5, 2012.
- <sup>14</sup>Moser, M. D., Merenich, J., Pal, S., and Santoro, R. J., "OH-radical imaging and velocity field measurements in a gaseous hydrogen/oxygen rocket," *29th Joint Propulsion Conference and Exhibit*, Joint Propulsion Conferences, American Institute of Aeronautics and Astronautics, June 1993.
- <sup>15</sup>Santoro, R. J., Pal, S., Woodward, R., and Schaaf, L., "Rocket Testing at University Facilities," *39th Aerospace Sciences Meeting and Exhibit*, Aerospace Sciences Meetings, American Institute of Aeronautics and Astronautics, Reno, NV, Jan. 2001, p. 16.
- <sup>16</sup>Hutt, J. and Cramer, J., "Advanced rocket injector development at the Marshall Space Flight Center," *Space Programs and Technologies Conference*, SPACE Conferences & Exposition, American Institute of Aeronautics and Astronautics, Sept. 1996.
- <sup>17</sup>Schumaker, S. A. and Driscoll, J. F., "Coaxial turbulent jet flames: Scaling relations for measured stoichiometric mixing lengths," *Proceedings of the Combustion Institute*, Vol. 32, No. 2, 2009, pp. 1655–1662.

<sup>18</sup>Clemens, N. T., "Flow Imaging," *Encyclopedia of Imaging Science and Technology*, 2002.

<sup>19</sup>Koban, W., Koch, J. D., Hanson, R. K., and Schulz, C., "Toluene LIF at elevated temperatures: implications for fuel/air ratio measurements," *Applied Physics B*, Vol. 80, No. 2, 2005, pp. 147–150.

<sup>20</sup>Schulz, C. and Sick, V., "Tracer-LIF diagnostics: quantitative measurement of fuel concentration, temperature and fuel/air ratio in practical combustion systems," *Progress in Energy and Combustion Science*, Vol. 31, No. 1, 2005, pp. 75–121.

<sup>21</sup>Villermaux, E. and Rehab, H., "Mixing in coaxial jets," *Journal of Fluid Mechanics*, Vol. 425, 2000, pp. 161–185.

<sup>22</sup>Schumaker, S. A. and Driscoll, J. F., "Mixing Lengths of Coaxial Jets in a Rocket Combustor Configuration Using Acetone PLIF," *43rd AIAA/ASME/SAE/ASEE Joint Propulsion Conference & Exhibit*, Joint Propulsion Conferences, American Institute of Aeronautics and Astronautics, Cincinnati, OH, July 2007.

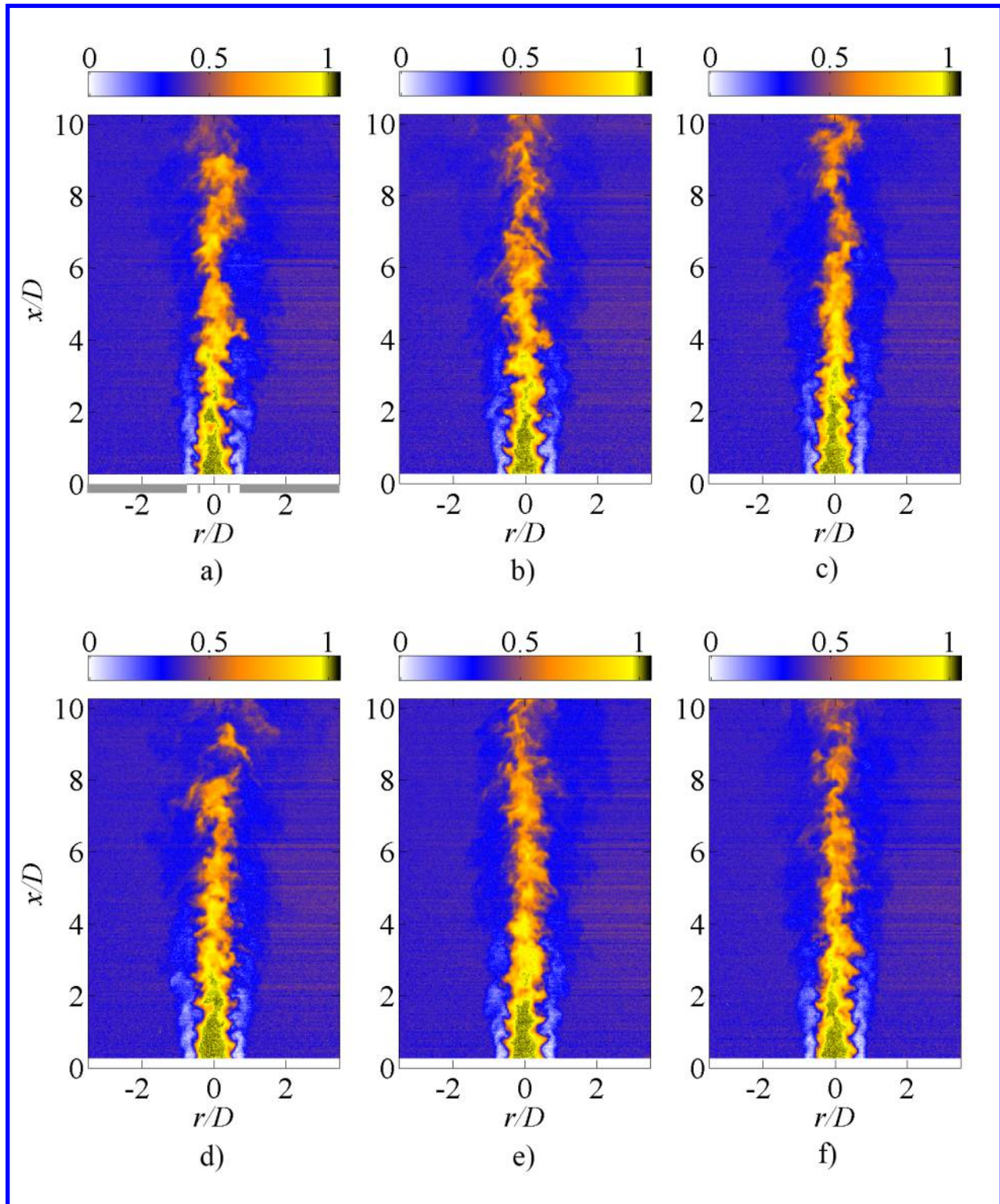


Figure 6. Set of consecutive instantaneous Toluene PLIF images for a case without side jets ( $S = 1.43$  and  $R = 1$ ). The position of coaxial injector is shown in a). Images show mole fraction of the inner stream gas.

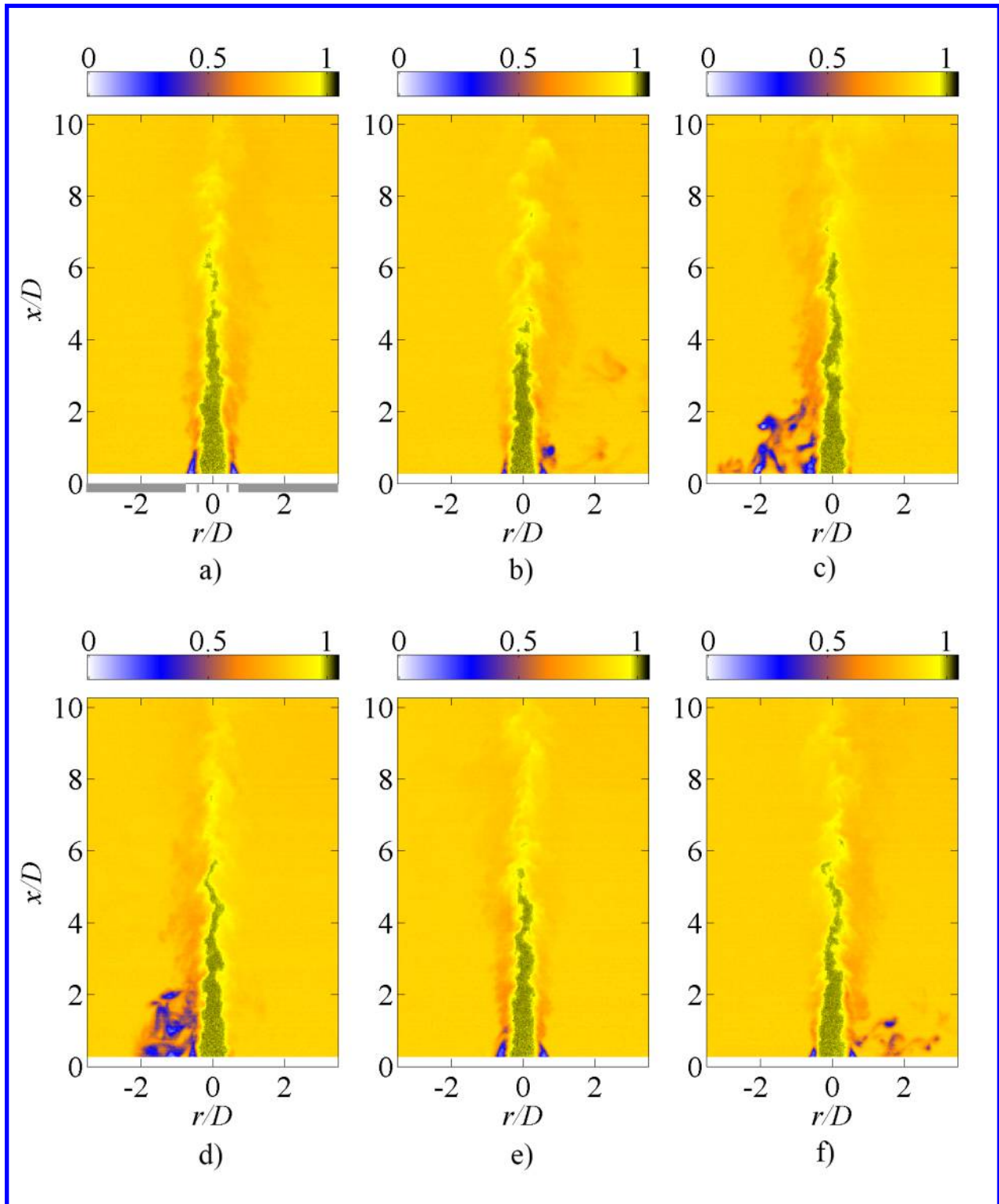


Figure 7. Set of consecutive instantaneous Toluene PLIF images for a case with side jets ( $S = 6.99$  and  $R = 6$ ). The position of coaxial injector is shown in a). Images show mole fraction of the inner stream gas.

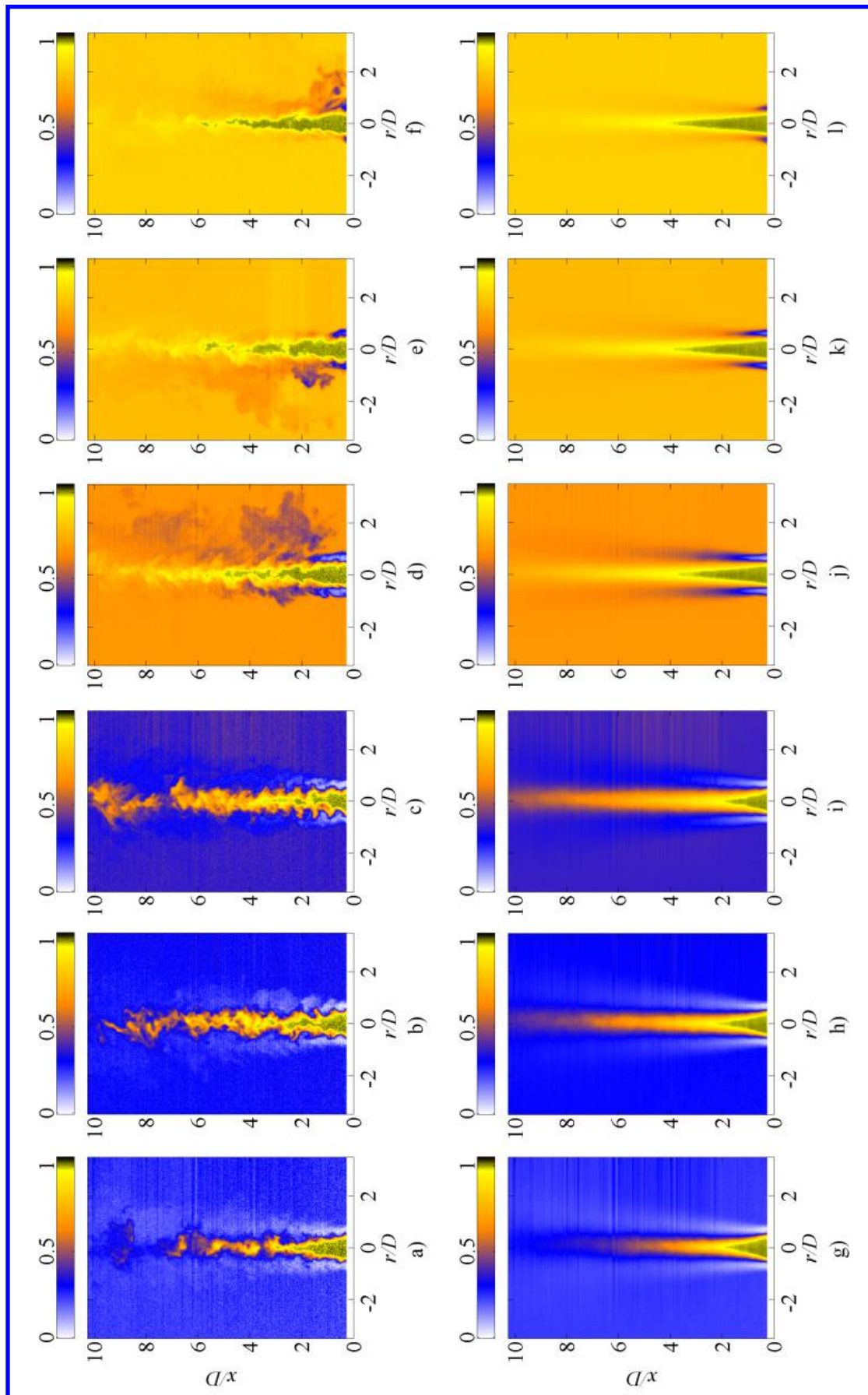


Figure 8. Toluene PLIF images for a constant  $S = 1.43$  and  $R$  increasing from left to right. a) to f) are instantaneous and g) to l) are corresponding average images for cases with  $R = 0.5, 0.7, 1, 3.5, 6$  and  $9$  respectively. Images show mole fraction of the inner stream gas.

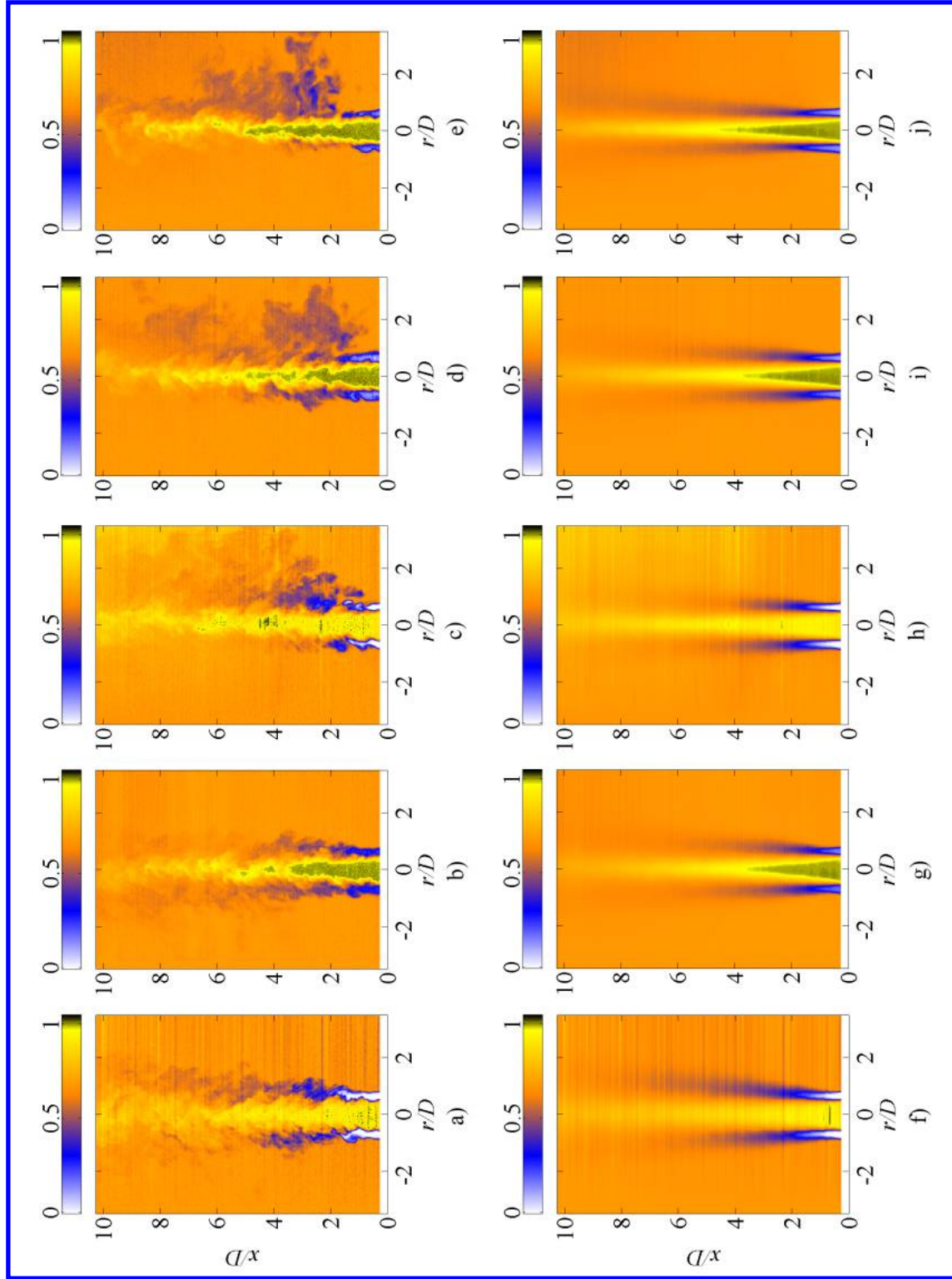


Figure 9. Toluene PLIF images for a constant  $R = 3.5$  and  $S$  increasing from left to right. a) to e) are instantaneous and f) to j) are corresponding average images for cases with  $S = 0.14, 0.70, 1, 1.43$  and  $6.99$  respectively. Images show mole fraction of the inner stream gas.

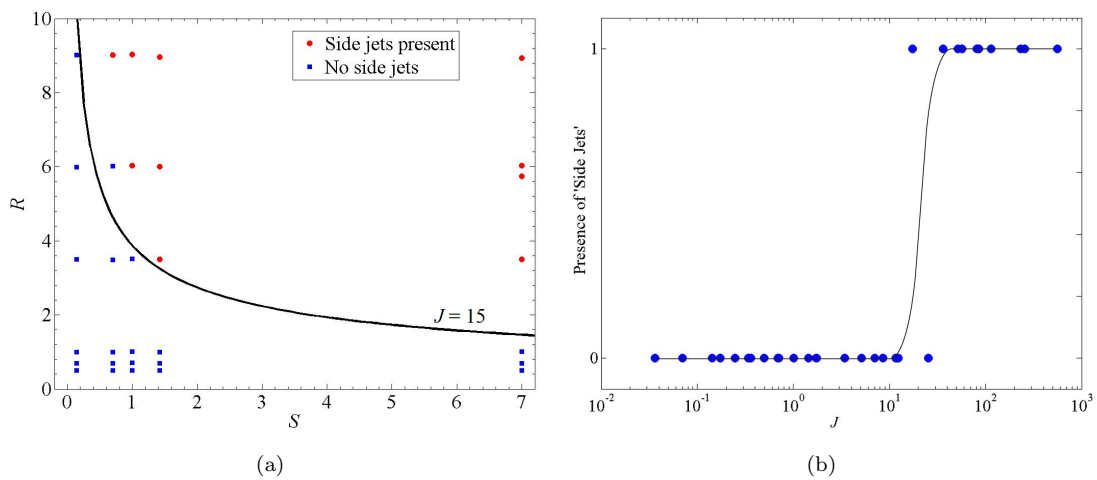


Figure 10. (a) Map showing the different density and velocity ratios considered for the non-reacting cases. Circular points in red are the cases where side jets were observed. A line of constant  $J$  ( $J = 15$ ) separates regimes with and without observed side jets. (b) Plot showing the presence of side jets at different momentum flux ratios. Values of 0 and 1 on the vertical axis represent the absence and presence of side jets, respectively. Black line shows the general trend.

**This article has been cited by:**

1. Abhinav Dasari, Mirko Gamba Variation of Dominant Instability Mode with Fuel Configuration in an Inverted Coaxial Injector .  
[Citation] [PDF] [PDF Plus]
2. Abhinav Dasari, Logan W. White, Mirko Gamba Investigation of Instability Mechanisms in a Laboratory Scale GH<sub>2</sub>/GO<sub>2</sub> Combustor . [Citation] [PDF] [PDF Plus]